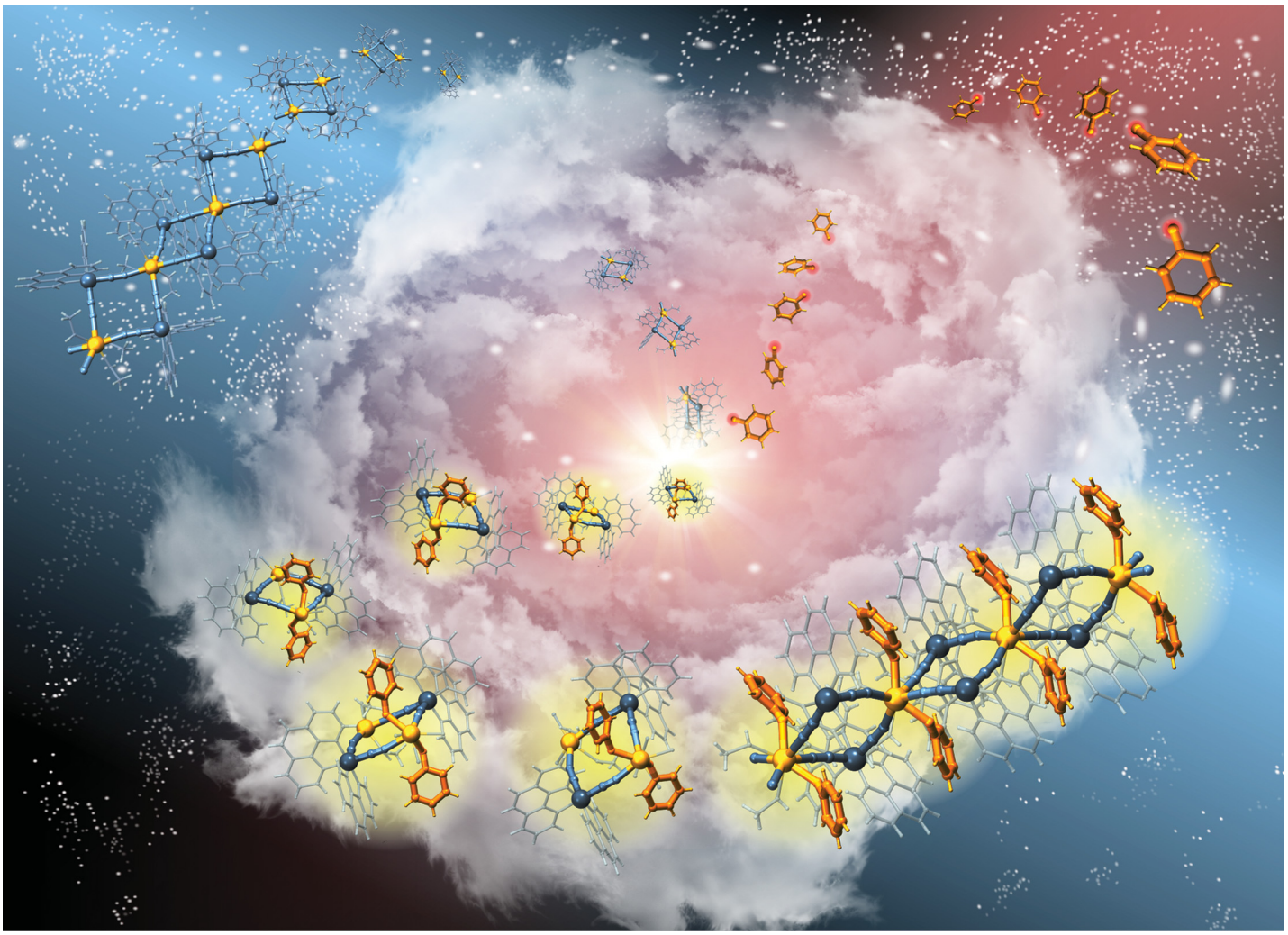

Showcasing research from Multifunctional Luminescent Materials Group of the Faculty of Chemistry, Jagiellonian University in Kraków, Poland.

Neutral dicyanidoferrate(II) metalloligands for the rational design of dysprosium(III) single-molecule magnets

Dicyanidobis(aromatic α,α′-diimine) Fe(II) complexes efficiently constrain the equatorial plane of Dy(III) centres by forming chains of vertex-sharing $\{Dy_2Fe_2\}$ squares. This opens the pathway for controlling the lanthanide magnetic anisotropy by placing organic *N*-oxides at axial positions of 4f metal complexes.

As featured in:

See Szymon Chorazy *et al.*, *Chem. Commun.*, 2022, **58**, 6381.

ROYAL SOCIETY OF CHEMISTRY

rsc.li/chemcomm

Registered charity number: 207890

ChemComm

COMMUNICATION

View Article Online
View Journal | View Issue

Cite this: *Chem. Commun.*, 2022, 58, 6381

Received 19th April 2022,
Accepted 3rd May 2022

DOI: 10.1039/d2cc02238a

rsc.li/chemcomm

Neutral dicyanidoferrate(II) metalloligands for the rational design of dysprosium(III) single-molecule magnets†

Michal Liberka, Mikolaj Zychowicz, Wiktor Zychowicz and Szymon Chorazy *

Diamagnetic *cis*-dicyanidoferrate(II) complexes bearing blocking aromatic diimines, *cis*-$[Fe^{II}(CN)_2(L_{NN})_2]^0$ (L_{NN} = 2,2′-bipyridine, 1,10′-phenanthroline) serve as metalloligands to Dy^{III} centres leading to a rigid cyanido-bridged chain of vertex-sharing $\{Dy^{III}_2Fe^{II}_2\}$ squares which constrains the equatorial plane of embedded 4f metal ions. This results in a novel convenient route to rationally designed single-molecule magnets as the magnetic anisotropy of Dy^{III} centres can be efficiently generated by inserting aromatic *N*-oxide ligands on labile axial positions.

Magnetic materials play a vital role in our life due to the applications in data storage, electric motors, power generation and conversion, refrigeration, and medical treatment.[1] In this context, increasing interest is given to molecular nanomagnets called Single-Molecule Magnets (SMMs) that reveal the slow magnetic relaxation resulting in a hysteresis loop of molecular origin.[2] Thus, they should revolutionize the fields of data storage,[3] spintronics,[4] and quantum computing.[5]

Lanthanide (Ln) ions arouse primary interest in the field of SMMs as they show strong magnetic anisotropy being the result of spin–orbit coupling and crystal-field effects.[6] They offer further functionalization of SMMs due to the efficient luminescence and softness of the crystal lattice.[7] The design principles for maximized anisotropy of 4f metal ions are related to the type of the f-electron density distribution for the preferred highest m_J state.[8] Oblate-type ions, *e.g.* Dy^{3+}, need the axial alignment of charged ligands to minimize the energy of $m_J = J$ state while prolate-type ions, *e.g.* Er^{3+}, require the equatorial alignment of charged ligands.[9] These rules, often supported by high complex symmetry,[2a,8b] are used for the design of Ln-SMMs. Among them, the most impressive results were found for Dy^{III} centres exhibiting huge anisotropy in sandwich-like organometallic complexes.[10] Their disadvantage lies in weak stability to chemical stimuli which is important for processing into devices.[3] This can be overcome using strategies based on coordination chemistry. The equatorial plane of the Dy^{III} centre can be constrained by weakly coordinating ligands enabling the introduction of ligands with charged donor atoms to the axial positions.[2c,8b] Besides the application of multidentate ligands controlling the whole coordination sphere,[11] this strategy was realized by two main routes. The first one employs solvent molecules occupying the equatorial plane and expanded organic *P*-/*N*-/alkyl-/aryl-oxides placed on the axial positions.[9a,12] The second one explores macrocyclic ligands constraining the equatorial plane which leaves the axial positions for oxide-type ligands.[13] In this regard, there is a continuous need for novel pathways towards Dy-SMMs exploring the axially and equatorially positioned ligands. We have undertaken this challenge exploiting cyanido complexes of transition metals which are efficient metalloligands for Ln-SMMs with luminescent, SHG-active, or proton-conductive properties.[14] Cyanido complexes used alone can induce moderate SMM property due to long Ln^{III}-*N*(cyanido) bond lengths. However, they can provide a rigid backbone for the f- or d-block metal counter-ions,[15] which can be used for constraining the equatorial plane of the Dy^{III} coordination sphere. To achieve this, we screened polycyanidometallates looking for a candidate with a sufficient number of cyanido ligands for bridging to 4f metal ion, being also suitably expanded to block the equatorial plane of Ln^{3+} ions, leaving space for axially aligned ligands. We found that these prerequisites are provided by *cis*-dicyanidoferrate(II) complexes bearing aromatic diimines, $[Fe^{II}(CN)_2(L_{NN})_2]^0$ (L_{NN} = 2,2′-bipyridine = bpy, 1,10′-phenanthroline = phen).[16] Here, we report four bimetallic coordination chains, $\{Dy^{III}(MeOH)_4[Fe^{II}(CN)_2(L_{NN})_2]_2\}(CF_3SO_3)_3 \cdot n$MeOH (**1**, L_{NN} = bpy, n = 1; **2**, L_{NN} = phen, n = 5) and $\{Dy^{III}(pyNO)_2(MeOH)_2[Fe^{II}(CN)_2(L_{NN})_2]_2\}(CF_3SO_3)_3 \cdot n$MeOH (**3**, L_{NN} = bpy, n = 0.5; **4**, L_{NN} = phen, n = 1.5). They are built of $\{Dy^{III}_2Fe^{II}_2\}$ squares that constrain the equatorial plane of Dy^{III} centres opening the way

Faculty of Chemistry, Jagiellonian University, Gronostajowa 2, 30-387 Krakow, Poland. E-mail: chorazy@chemia.uj.edu.pl

† Electronic supplementary information (ESI) available: Experimental section, IR spectra, TGA, detailed structural analysis, detailed *dc*/*ac* magnetic analyses, details concerning the relACs programme, details of the *ab initio* calculations. CCDC 2123814 (**1**), 2123813 (**2**), 2123815 (**3**) and 2123812 (**4**). For ESI and crystallographic data in CIF or other electronic format see DOI: https://doi.org/10.1039/d2cc02238a

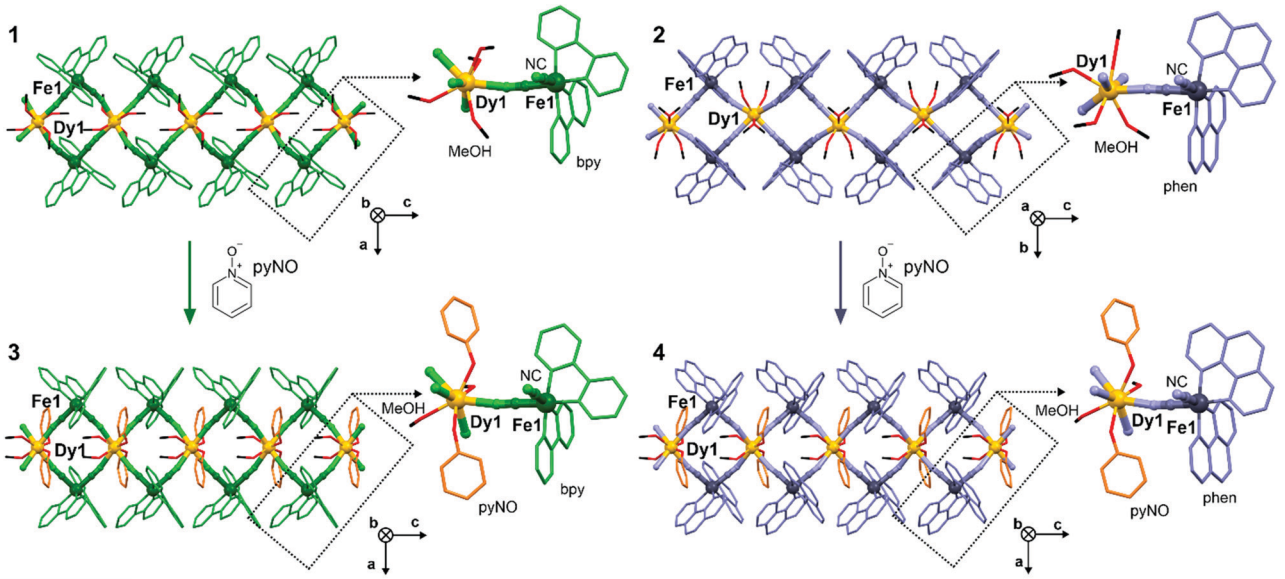

Fig. 1 The views of cyanido-bridged chains of vertex-sharing $\{Dy^{III}_2Fe^{II}_2\}$ squares of **1–4** shown together with respective molecular building units.

to generate the SMM behaviour by the insertion of pyridine *N*-oxide (pyNO) ligands on the axial positions of Dy^{III} which was investigated using X-ray diffraction data and dc/ac magnetic characteristics analysed by a newly developed relACs programme supported by the *ab initio* calculations.

Crystals of **1** and **2** were obtained by the self-assembly of $Dy^{III}(CF_3SO_3)_3$ with *cis*-$[Fe^{II}(CN)_2(bpy/phen)_2]$ in the MeOH/MeCN solution. Their basic characterization using CHNS analysis, IR spectra and TGA (see Experimental section and Fig. S1 and S2, ESI†) was followed by a single-crystal X-ray diffraction analysis (Fig. 1 and Fig. S3–S5, Tables S1–S6, S11–S15, ESI†). **1** and **2** crystallize in the *C*2/*c* space group (Tables S1 and S2, ESI†) and are composed of cyanido-bridged chains of vertex-sharing $\{Dy^{III}_2Fe^{II}_2\}$ squares crystallizing with $CF_3SO_3^-$ ions and MeOH of crystallization (Fig. S3–S5, ESI†). Each Dy^{III} centre coordinates four CN^- ligands from four neighbouring $[Fe^{II}(CN)_2(L_{NN})_2]$ complexes, while each Fe^{II} site links two different 4f metal ions (Fig. 1). As the convergent *cis*-dicyanido complexes were used, this results in the $\{Dy^{III}_2Fe^{II}_2\}$ squares sharing the Dy^{III} centres. The coordination sphere of 4f metal centres is completed by MeOH ligands, lying above and below the equatorial plane of Dy–NC–Fe linkages. The Dy^{III} centre and surrounding Fe^{II} sites do not lie in the ideal plane as the neighbouring squares are twisted (Fig. S3–S5 and Table S11, ESI†). The Dy^{III} centres are dodecahedral in **2** or of a mixed geometry between dodecahedral and square antiprismatic in **1** (Tables S3–S6 and S12–S15, ESI†). The Dy–N(CN^-) and Dy–O(MeOH) distances vary in the range of 2.39–2.47 Å in **1** and **2** (Tables S3–S6, ESI†). Each Fe^{II} site coordinates two diimine ligands that protrude from a coordination skeleton stabilizing the structure by interchain π–π stacking (Fig. S8, ESI†). The addition of pyNO to the same solution as used for **1** and **2** gives the crystals of **3** and **4**, respectively (see Experimental section). **3** and **4** crystallize in the *Pccn* space group but they are similar to **1** and **2** being built of CN^--bridged chains of $\{Dy^{III}_2Fe^{II}_2\}$ squares crystallizing with $CF_3SO_3^-$ ions and MeOH molecules (Fig. 1 and Fig. S3, S6, S7, Tables S1–S2, S7–S15, ESI†). The difference lies in pyNO ligands attached to the Dy^{III} centres. Each 4f metal ion coordinates two pyNO ligands replacing two out of four MeOH ligands present in the Dy^{III} complexes in **1** and **2**. They are located on the axial positions of square-antiprismatic Dy^{III} centres, above and below the equatorial plane given by four Dy–NC–Fe linkages. The Dy–O(pyNO) distances are shorter (*ca.* 2.36 Å) than Dy–O(MeOH) and Dy–N(CN^-) ones (2.42–2.45 Å, Tables S7–S10, ESI†). However, its vertical alignment is not perfectly axial as depicted by the O(pyNO)–Dy–O(pyNO) angle, 124.6(2)° (**3**) and 127.9(3)° (**4**), which is related to the twist between neighbouring $\{Dy^{III}_2Fe^{II}_2\}$ squares. The alignment of pyNO ligands is controlled by intrachain π–π stacking with the L_{NN} ligands which are also involved in interchain π–π interactions (Fig. S6–S8, ESI†). The validity of the structural models were confirmed by the P-XRD (Fig. S9, ESI†).

The direct-current (dc) magnetism for **1–4** is similar (Fig. S10, ESI†), including the decrease of the $\chi_M T$ product upon cooling related to the thermal depopulation of higher-lying m_J states of the ground Dy^{III} multiplet as well as the featureless course of the $M(H)$ plots at 1.8 K. These properties can be assigned to the single-ion effects of the Dy^{III} complexes which are magnetically isolated (J of *ca.* −0.07 cm^{-1} as determined for **3**, see Fig. S10, ESI†) due to their separation in the crystal lattice by diamagnetic Fe^{II} centres.[16] The alternate-current (ac) magnetism of **1–4** is shown in Fig. 2 and Fig. S11–S22, Tables S16–S18 (ESI†). Under zero-dc-field, **1** and **2** do not show a distinct slow magnetic relaxation effect as only the onsets of χ_M'' susceptibility were detected in the high-frequency region (Fig. 2a and b, the insets). However, the χ_M'' signals in **1** and **2** increase and shift to lower frequencies upon the applied dc field (Fig. S11 and S13, ESI†). Under the optimal dc field of 800 Oe, the ac susceptibility was investigated for variable T showing magnetic relaxations below 4 K (**1**) or 3 K (**2**) (Fig. S12 and S14, ESI†). Only for **1**, the accessible range of relaxation times, determined using the Debye model, enables the analysis of overall relaxation by

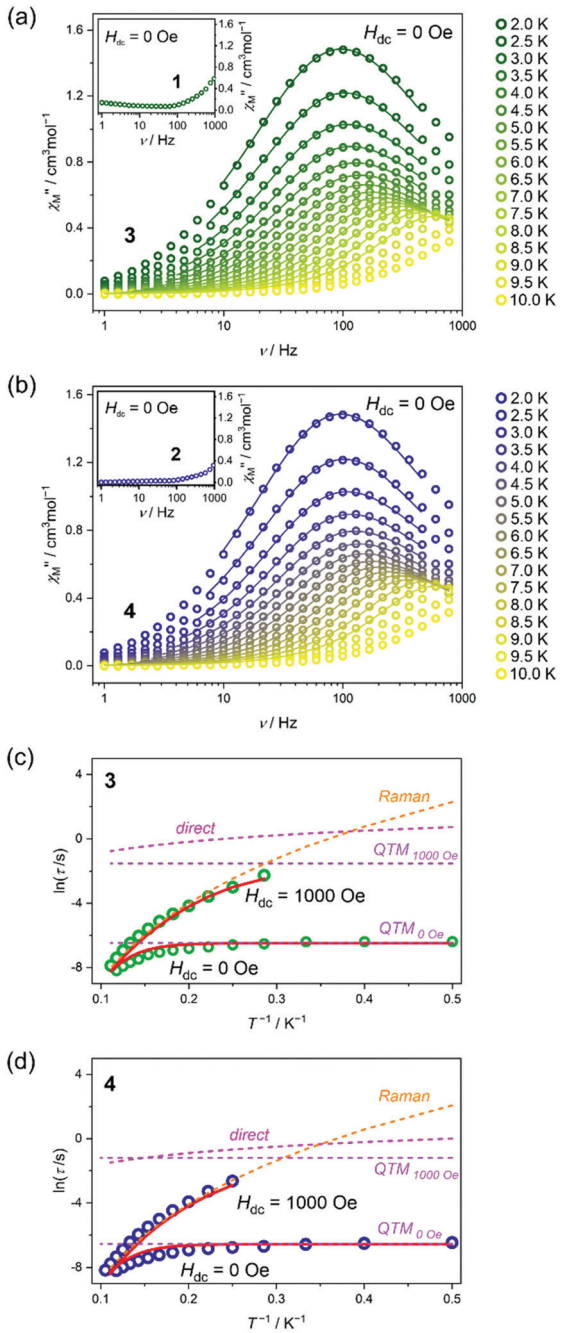

Fig. 2 Alternate-current (ac) magnetism of **1–4**: the frequency dependences of out-of-phase susceptibility, χ'', for the 2–10 K range at H_{dc} = 0 Oe for **3** (a) and **4** (b), together with the fitting to the Debye model (solid lines), compared with the ac signals at H_{dc} = 0 Oe for **1** and **2** (the insets), and the *T*-dependences of relaxation time at H_{dc} = 0 Oe and H_{dc} = 1000 Oe for **3** (c) and **4** (d). In c and d, circle points show the experimental data, solid lines show the best-fit curves obtained taking into account the combined contribution from direct, Raman, and QTM processes while dashed lines show the separate contributions from each process.

taking into account three processes: direct, Raman, and QTM (Fig. S11–S22, ESI†). The best-fit parameters prove that the *H*-induced magnetic relaxation in **1** is dominated by the Raman process in the 2–4 K range while by the QTM below 2 K (Fig. S12 and Tables S17, S18, ESI†). On the contrary, compounds **3** and **4** exhibit distinct maxima on the $\chi_M''(\nu)$ plots under zero-dc-field (Fig. 2a and b). They appear almost at the same frequency in the 2–4 K range due to the strong QTM. Then, they shift to higher frequencies being detectable to 10 K in the 1–1000 Hz range. The full set of ac magnetic data for **3** and **4**, including field-dependences at 5 K as well as *T*-dependences at zero and optimal (1 kOe) dc fields, was fitted using the Debye model (Fig. S15–S20, ESI†). The extracted relaxation times were analysed using the simultaneous, 3-D fitting based on all obtained curves, $\tau(T, H)$, taking into account direct, Raman, and QTM processes (Fig. 2c, d and Fig. S21, ESI†). All analyses were realized by a purposefully developed relACs programme that enables the fitting of ac data to various models and further 3-D fitting of $\tau(T, H)$ curves with the visualization of contributions from relaxation processes which was shown for **3–4** in Fig. 2c and d (for details see ESI,† Fig. S23). We also performed an alternative fit taking into account the Orbach relaxation with a fixed energy barrier, ΔE, taken from the *ab initio* calculations (Fig. S22, ESI†). The obtained results are consistent with the former fitting, which confirms the major role of the Raman process. The best-fit parameters reproduce well the experiment indicating that the energy barriers of Orbach relaxation of 80.3 and 85.9 cm^{-1} for **3** and **4**, respectively, can be postulated (Fig. S15–S22 and Table S16, ESI†). Despite these values, magnetic relaxation is observed only up to 10 K which is due to the Raman relaxation becoming the main pathway above 7 or 3 K for zero and optimal dc fields, respectively (Fig. 2c, d and Table S17, ESI†). Slightly better SMM features were found for **4** which is due to the larger O(pyNO)–Dy–O(pyNO) angle and the shorter Dy–O(pyNO) distance increasing the ΔE, contributing to quenching of other relaxation routes, *e.g.* QTM.

Insight into the transition from weak to distinct SMM features from **1–2** to **3–4** is given by *ab initio* calculations of a CASSCF/RASSI/SINGLE_ANISO type (Fig. 3 and Tables S19–S21, Fig. S24, and the comment in ESI†). They show that the ground Dy^{III} multiplets in **1–2** consist of the mixture of $|J, m_J\rangle$ states of $|15/2, \pm 15/2\rangle$ (main contribution) and $|15/2, \pm 11/2\rangle$ (Table S20 and S21, ESI†). The significant mixing for the ground states in **1–2** explains the strong QTM effect and the lack of field-free slow magnetic relaxation. However, the SMM effect appears in **1–2** under a dc field, and, for **1**, the energy of

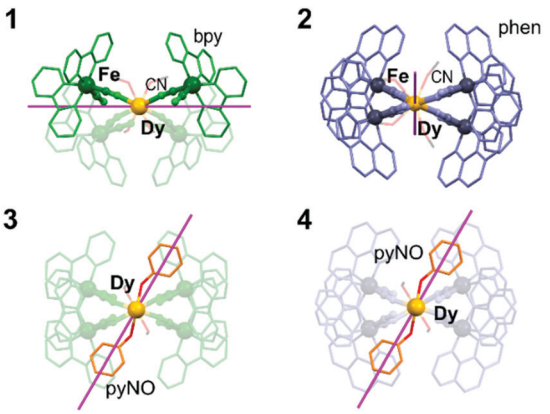

Fig. 3 The alignment of easy magnetic axes of Dy complexes in **1–4**, determined by the *ab initio* method (Tables S20 and S21, ESI†).

the first excited m_J level of 60.0 cm^{-1} can serve as the estimation of the ΔE of Orbach relaxation, considered in the broadened fit to the ac data (as for **3–4**, see Table S16, ESI† and above). The insertion of pyNO in **3–4** improves the magnetic axiality as the related ground Dy^{III} multiplets consist of almost pure $|15/2, \pm 15/2\rangle$ states with the admixtures of other states below 0.8% (Tables S20 and S21, ESI†). This gives the g_z values > 19.8, higher than for **1–2**, but non-negligible transversal components remain. It explains the observation of field-free SMM behaviour with the not fully quenched QTM. The energies of the first excited m_J levels in **3–4** can be connected with the Orbach energy barriers; however, it is not crucial as the Raman relaxation dominates. The dramatic changes in anisotropy in **3–4** are proved by the modified alignment of magnetic easy axes (Fig. 3 and Fig. S24, ESI†). In **1–2**, they are arranged in the plane formed by four cyanido bridges which provide the most negative charges. In **3–4**, the easy axes deflect toward the direction of pyNO ligands proving that they are responsible for enhanced SMM features.

We report a convenient strategy for the design of Dy^{III} SMMs based on the application of *cis*-dicyanidoferrate(II) complexes blocked by diimine ligands. Despite their overall zero charges, unusual among cyanidometallates,[14] they serve as metalloligands for Dy^{3+} ions leading to the rigid chain structure that constrains the equatorial plane of the 4f metal centre. As a result, to the axial positions of the Dy^{III} complex, primarily occupied by solvent molecules, one can introduce the organic-oxide-type ligands generating SMM behaviour. This strategy is an alternative to typical approaches using weakly coordinated solvents or macrocyclic ligands occupying the equatorial plane of the Dy^{III} centres.[12,13] As ligands on both metal sites can be modified, or the Fe^{II} centres can be replaced with other d-block metals,[17] this approach opens the route to Dy-SMMs revealing optimized magnetic anisotropy, *e.g.* by amending the coordination geometry or the axial ligand field,[12] and further functionalized towards luminescent and chiro-optical properties. We will search for more rigid cyanido-bridged skeletons leaving two axially positioned solvent molecules for incorporation of charged organic ligands.

This work was financed by the National Science Centre, Poland the OPUS-15 project no. 2018/29/B/ST5/00337. M. Z. acknowledges the Polish Ministry of Science and Higher Education for the Diamond Grant (DI2018 017948).

Conflicts of interest

There are no conflicts to declare.

Notes and references

1 (*a*) O. Gutfleisch, M. A. Willard, E. Brück, C. H. Chen, S. G. Sankar and J. P. Liu, *Adv. Mater.*, 2011, **23**, 821; (*b*) A. V. Kimel and M. Li, *Nat. Rev. Mater.*, 2019, **4**, 189.
2 (*a*) N. Ishikawa, M. Sugita, S. Koshihara and Y. Kaizu, *J. Am. Chem. Soc.*, 2003, **125**, 8694; (*b*) S. K. Gupta and R. Murugavel, *Chem. Commun.*, 2018, **54**, 3685; (*c*) F.-S. Guo, B. M. Day, Y.-C. Chen, M.-L. Tong, A. Mansikkamäki and R. A. Layfield, *Science*, 2018, **362**, 1400.
3 M. Mannini, F. Pineider, P. Sainctavit, C. Danieli, E. Otero, E. Sciancelepore, A. M. Talarico, M.-A. Arrio, A. Cornia and D. Gatteschi, *Nat. Mater.*, 2009, **8**, 194.
4 A. Candini, S. Klyatskaya, M. Ruben, W. Wernsdorfer and M. Affronte, *Nano Lett.*, 2011, **11**, 2634.
5 A. Gaita-Arino, F. Luis, S. Hill and E. Coronado, *Nat. Chem.*, 2019, **11**, 301.
6 (*a*) D. N. Woodruff, R. E.-P. Winpenny and R. A. Layfield, *Chem. Rev.*, 2013, **113**, 5510; (*b*) P. Zhang, L. Zhang and J. Tang, *Dalton Trans.*, 2015, **44**, 3923; (*c*) Z. Zhu, M. Guo, X.-L. Li and J. Tang, *Coord. Chem. Rev.*, 2019, **378**, 350; (*d*) Z. Zhu, X.-L. Li, S. Liu and J. Tang, *Inorg. Chem. Front.*, 2020, **7**, 3315.
7 (*a*) F. Pointillart, B. Le Guennic, S. Golhen, O. Cador, O. Maury and L. Ouahab, *Chem. Commun.*, 2013, **49**, 615; (*b*) Y. Xin, J. Wang, M. Zychowicz, J. J. Zakrzewski, K. Nakabayashi, B. Sieklucka, S. Chorazy and S. Ohkoshi, *J. Am. Chem. Soc.*, 2019, **141**, 18211; (*c*) J. Wang, J. J. Zakrzewski, M. Zychowicz, V. Vieru, L. F. Chibotaru, K. Nakabayashi, S. Chorazy and S. Ohkoshi, *Chem. Sci.*, 2021, **12**, 730; (*d*) R. Marin, G. Brunet and M. Murugesu, *Angew. Chem., Int. Ed.*, 2021, **60**, 1728.
8 (*a*) J. D. Rinehart and J. R. Long, *Chem. Sci.*, 2011, **2**, 2078; (*b*) J.-L. Liu, Y.-C. Chen and M.-L. Tong, *Chem. Soc. Rev.*, 2018, **47**, 2431.
9 (*a*) Y.-C. Chen, J.-L. Liu, L. Ungur, J. Liu, Q.-W. Li, L.-F. Wang, Z.-P. Ni, L. F. Chibotaru, X.-M. Chen and M.-L. Tong, *J. Am. Chem. Soc.*, 2016, **138**, 2829; (*b*) P. Zhang, L. Zhang, C. Wang, S. Xue, S.-Y. Lin and J. Tang, *J. Am. Chem. Soc.*, 2014, **136**, 4484; (*c*) Z. Zhu, Y.-Q. Zhang, X.-L. Li, M. Guo, J. Lu, S. Liu, R. A. Layfield and J. Tong, *CCS Chem.*, 2021, **3**, 338.
10 B. M. Day, F.-S. Guo and R. A. Layfield, *Acc. Chem. Res.*, 2018, **51**, 1880.
11 J. Liu, Y.-C. Chen, J.-L. Liu, V. Vieru, L. Ungur, J.-H. Jia, L. F. Chibotaru, Y. Lan, W. Wernsdorfer, S. Gao, X.-M. Chen and M.-L. Tong, *J. Am. Chem. Soc.*, 2016, **138**, 5441.
12 (*a*) S. K. Gupta, T. Rajeshkumar, G. Rajaraman and R. Murugavel, *Chem. Sci.*, 2016, **7**, 5181; (*b*) Y.-S. Ding, N. F. Chilton, R. E.-P. Winpenny and Y.-Z. Zheng, *Angew. Chem., Int. Ed.*, 2016, **55**, 16071; (*c*) A. B. Canaj, M. K. Singh, C. Wilson, G. Rajaraman and M. Murrie, *Chem. Commun.*, 2018, **54**, 8273.
13 (*a*) A. B. Canaj, S. Dey, E. R. Marti, C. Wilson, G. Rajaraman and M. Murrie, *Angew. Chem., Int. Ed.*, 2019, **58**, 14146; (*b*) A. B. Canaj, S. Dey, C. Wilson, O. Cespedes, G. Rajaraman and M. Murrie, *Chem. Commun.*, 2020, **56**, 12037; (*c*) Z. Zhu, C. Zhao, T. Feng, X. Liu, X. Ying, X.-L. Li, Y.-Q. Zhang and J. Tang, *J. Am. Chem. Soc.*, 2021, **143**, 10077.
14 (*a*) S. Chorazy, J. Wang and S. Ohkoshi, *Chem. Commun.*, 2016, **52**, 10795; (*b*) M. Andruh, *Chem. Commun.*, 2018, **54**, 3559; (*c*) J. Wang, J. J. Zakrzewski, M. Heczko, M. Zychowicz, K. Nakagawa, K. Nakabayashi, B. Sieklucka, S. Chorazy and S. Ohkoshi, *J. Am. Chem. Soc.*, 2020, **142**, 3970.
15 E. V. Alexandrov, A. V. Virovets, V. A. Blatov and E. V. Peresypkina, *Chem. Rev.*, 2015, **115**, 12286.
16 (*a*) I. Georgieva, A. J.-A. Aquino, N. Trendafilova, P. S. Santos and H. Lischka, *Inorg. Chem.*, 2010, **49**, 1634; (*b*) M. Liberka, K. Boidachenko, J. J. Zakrzewski, M. Zychowicz, J. Wang, S. Ohkoshi and S. Chorazy, *Magnetochemistry*, 2021, **7**, 79.
17 T. Abe and K. Shinozaki, *Inorg. Chem.*, 2005, **44**, 849.

